

Fluidization of spherical versus elongated particles - experimental investigation using X-ray tomography

Mema, Ivan; Wagner, Evert C.; van Ommen, J. Ruud; Padding, Johan T.

DOI

[10.1016/j.cej.2020.125203](https://doi.org/10.1016/j.cej.2020.125203)

Publication date

2020

Document Version

Final published version

Published in

Chemical Engineering Journal

Citation (APA)

Mema, I., Wagner, E. C., van Ommen, J. R., & Padding, J. T. (2020). Fluidization of spherical versus elongated particles - experimental investigation using X-ray tomography. *Chemical Engineering Journal*, 397, Article 125203. <https://doi.org/10.1016/j.cej.2020.125203>

Important note

To cite this publication, please use the final published version (if applicable). Please check the document version above.

Copyright

Other than for strictly personal use, it is not permitted to download, forward or distribute the text or part of it, without the consent of the author(s) and/or copyright holder(s), unless the work is under an open content license such as Creative Commons.

Takedown policy

Please contact us and provide details if you believe this document breaches copyrights. We will remove access to the work immediately and investigate your claim.



Fluidization of spherical versus elongated particles - experimental investigation using X-ray tomography



Ivan Mema^{a,*}, Evert C. Wagner^b, J. Ruud van Ommen^b, Johan T. Padding^a

^a Complex Fluid Processing, Department of Process and Energy, Delft University of Technology, Leeghwaterstraat 39, 2628 CB Delft, The Netherlands

^b Department of Chemical Engineering, Delft University of Technology, Van der Maasweg 9, 2629 HZ Delft, The Netherlands

HIGHLIGHTS

- X-ray tomography applied to fluidized bed of elongated particles.
- Comparison of fluidization characteristic between spherical and elongated particles.
- Bed of elongated particles shows more turbulent fluidization behavior.
- Bed of Geldart D spherical particles remains in constant slugging regime.
- Bed of elongated particles switches between slugging and turbulent fluidization.

ARTICLE INFO

Keywords:

Fluidization
X-ray tomography
Elongated particles
Slugging
Geldart D

ABSTRACT

In many industrial applications, particles used in fluidized bed clearly deviate from ideal spheres. This leads to an increasing need for better understanding and developing better simulation models for fluidization of non-spherical particles. So far, the literature is quite scarce when it comes to experimental results which can be used for validation of numerical models. Also, the exact difference in fluidization behavior between spherical and elongated particles in dense fluidizing conditions is not well understood. In this work, we apply X-ray tomography to compare the fluidization behavior of a bed of a Geldart D-type spherical particles of aspect ratio 4 to that of volume equivalent spherocylindrical particles for different gas velocities. Even though the beds of both spherical and elongated particles are operating in the slugging regime, due their size and high bed height to width ratio, we see clear differences in their fluidization behavior. Our results indicate that the bed of elongated particles is slugging less than the one with spherical particles. This is indicated by a lower average bubble size in the case of elongated particles, together with a higher bubble rise velocity. The bed of elongated particles has a considerably higher distribution of small and medium bubbles. The slug waiting time distribution and slug frequency distribution indicate that a bed of elongated particles periodically switches between slugging and turbulent fluidization, unlike the bed of spherical particles which remains in the constant slugging regime.

1. Introduction

Fluidized beds are irreplaceable equipment for the process industry, offering the best contact between a dispersed solid and continuous fluid phase. Fluidized beds have broad application, ranging from food-processing, waste disposal, coating, and chemical synthesis to energy production. Due to its important role in the chemical industry, fluidized beds have been the focus of numerous research in the past decades. However, a large fraction of this research focuses on a relatively smoothly bubbling fluidized beds with Geldart A or B particles. With such a versatile application of fluidized beds in industry, particles that

are being fluidized can have various shapes and sizes. With the rising need to switch to more sustainable and renewable material and energy sources, fluidized beds have found an important role in biomass processing. Typical biomass particles used in the process industry, such as wood chips, pellets and straw like material are not only characterized by an elongated shape but are also of considerably larger size than powder like materials which are typically used in fluidized beds. These large elongated particles have much more complex particle-particle interactions and experience additional orientation dependent hydrodynamic forces [1,2].

Fluidized beds with non-spherical particles have become a topic of

* Corresponding author.

E-mail address: i.mema@tudelft.nl (I. Mema).

<https://doi.org/10.1016/j.cej.2020.125203>

Received 5 February 2020; Received in revised form 21 April 2020; Accepted 22 April 2020

Available online 11 May 2020

1385-8947/ © 2020 The Author(s). Published by Elsevier B.V. This is an open access article under the CC BY license

(<http://creativecommons.org/licenses/by/4.0/>).

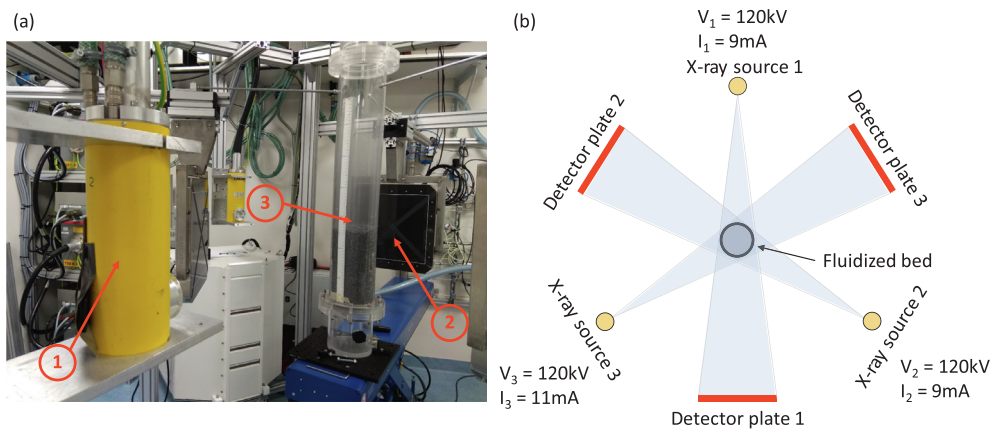


Fig. 1. (a) View of the fluidized bed column between the source and the detector plate, 1-X-ray source tube, 2-Detector plate, 3-Fluidized bed column. (b) Schematic of X-ray setup (top view).

research quite recently. There is already a large number of numerical investigations of such systems [2–6]. However, experimental studies are still quite scarce. Most experiments deal with pseudo 2D fluidized beds and are done using Particle Image Velocimetry (PIV) and/or Digital Image Analysis (DIA) [7–9]. However, in dense fluidized beds, such methods can only give insight into the near-wall region of the bed. To get insight into a full 3D fluidized bed is much more challenging, and requires more advanced non-intrusive 3D experimental techniques. One possible method is particle tracking. There are various methods of particle tracking techniques, the most famous one in fluidization is PEPT [10,11]. The magnetic particle tracking technique (MPT) [12] is a novel method, that was successfully applied to fluidized beds of elongated particles [13,14]. X-ray particle tracking is another method that was recently applied to investigate fluidization of binary mixtures of cylindrical and spherical particles [15,16]. Particle tracking is a powerful method that gives insight into time-averaged single particle features, such as orientation, occupancy and translation and rotation velocities.

Tomographic methods like electrical capacitance tomography [17–19] and X-ray tomography on the other hand, can give an overall picture of gas-solids distribution. X-ray tomography was one of the first non-intrusive 3D experimental techniques applied on fluidized beds [20–22]. Tomographic reconstruction is a unique method which is able to give insight into gas bubble size, shape and location in the fluidized bed. The bubble dynamics plays a significant role in the fluidization process as it is the main driving force for solids motion and also determines the contact surface between gas and solid phase. Therefore, understanding the bubble behavior inside a fluidized bed is crucial for determining its efficiency and for equipment optimization. So far, most of the research using X-ray tomography focused on bubbling fluidized beds. However due to the use of various types of particles, fluidized beds can operate in different regimes like slugging and turbulent fluidization [23]. This operating regime received considerably less attention compared to bubbling fluidization and most available findings are not of recent date [24–27]. Recently, a few more studies on slugging behavior in small diameter columns appeared [28–30]. However these focus only on Geldart A type powders. When it comes to Geldart D type particles, the only available models for estimating bubble properties have been developed by Baeyens and Geldart [24] and more recently by Agu et al. [31,32]. Venier et al. [33] looked into slugging fluidization of different type of particles, including Geldart D type, both experimentally and numerically. However these studies are limited to high bed height to diameter ratios.

In this work we investigate the fluidization behavior of a deep bed of Geldart D particles that is expected to operate in the slugging regime by means of X-ray tomography. We will compare fluidization properties of a bed containing spherical particles to one containing elongated,

spherocylindrical particles, for different gas velocities.

2. Experimental setup and methods

X-ray tomography (XRT) is a well established non-intrusive method for studying fluidized beds [34–37]. The main idea behind applying this method in fluidized bed investigation is to reconstruct the solid or gas fraction, based on the intensity of X-rays detected after passing through the fluidized bed. The 2D image reconstruction for horizontal cross sections of the fluidized bed in this work is done using the simultaneous algebraic reconstruction technique (SART) as defined in [21], implemented in the ASTRA Toolbox package. This technique has already been successfully applied in the same fluidized bed vessel with other particles [38]. More information about the measurement principles can be found in [21,39].

2.1. Fluidized bed and particles

In this work experiments were conducted in a perspex cylindrical column with an inner diameter of 14 cm and a height of 140 cm. The fluidized bed column is positioned inside the X-ray setup, surrounded by three X-ray sources placed at 120° around the column, as shown in Fig. 1. Each X-ray source is paired with a detector plate positioned on the opposite side, so that the column is in-between them. The X-ray sources used in this setup were YXLON Y.TU 160-D06 tubes with a maximum voltage of 150 kV and a maximum current of 12 mA. The used voltage and current depend on the investigated material and setup and have to be chosen such that the X-ray intensity is high enough to be detected after passing through the full bed but not exceed the upper limit of the detector after passing through an empty bed. The choice of X-ray source voltage and current used in this work is shown in Fig. 1 (b). The X-ray detector plates are Xineos-3131 with a sensitive area of $307 \text{ mm} \times 302 \text{ mm}$ and a resolution of 1548×1524 pixels. The dimensions of each pixel are $198 \mu\text{m} \times 198 \mu\text{m}$. The energy range in which the detectors can operate is from 40 kV to 120 kV. In this work we used a field of view of 1548×100 pixels in order to do measurements at an elevated rate of 200 frames per second.

Two types of particles were considered, spherical (aspect ratio 1, AR-1) and volume equivalent spherocylinders of aspect ratio 4 (AR-4). The particles were 3D printed by means of selective laser sintering and made of alumide, a 3D printing material which is a mixture of nylon and aluminium fine powder. The obtained particles can be classified as Geldart D particles and all their properties are listed in Table 1. In all experiments, the total particle mass in the bed was kept constant at 3.3 kg. The ratios between the initial bed height and the column diameter are 1.82 and 1.85 for AR-1 and AR-4 particles, respectively, so these fluidized beds are categorized as deep beds. Deep beds of Geldart

Table 1
Particle properties.

Parameter	AR-1	AR-4
Particle mass of the bed	3.3 kg	3.3 kg
Initial bed height	25.5 cm	26 cm
Particle length [L]	–	12 mm
Particle diameter [2R]	5.3 mm	3 mm
Particle material	Alumide	Alumide
Particle density	1442 kg/m ³	1442 kg/m ³
Mass of particle	0.112 g	0.112 g
Minimum fluidization velocity [U _{mf}]	1.58 m/s	1.7 m/s

D particles are expected to operate in the slugging regime [23].

2.2. Calibration and phantom reconstruction

Image reconstruction was done using two point calibration with the empty and full bed as upper and lower limits to the signal. Separate calibration has been performed for the spherical and elongated particles. The quality of the reconstruction is tested using phantoms of known dimensions. Cylindrical phantoms of 5.2 cm and 2 cm diameter were inserted vertically in the packed bed of particles. Images of the reconstructed horizontal cross sections of the phantoms and their estimated sizes are shown in Fig. 2. The reconstructed image is presented on a 100 × 100 cell grid, where the gray area indicates space around the column, black color refers to areas of the bed packed with particles, while white color responds to reconstructed voids (bubbles). The estimations of the phantom sizes are accurate: in the worst case it overestimates the real size by only 6.34%. Based on the phantom reconstructions, the threshold chosen for distinguishing bubbles from a packed area of the bed is 0.09 (relative between minimum and maximum intensity value). As the particles used in this investigation are quite coarse (see Table 1), the voids presented inside the packing can also be quite large and they can lead to a distortion of the reconstructed phantom shape and overestimation of its size. This is particularly the case for the large phantom which, due to its higher contact surface with the particles around it, has a large relative overestimation of its size. The 2 cm phantom is reconstructed successfully in all cases and therefore we set it as the minimum size of the bubbles that can be reconstructed with certainty. All bubbles smaller than 2 cm will be neglected in the further analysis.

3. Results

In this section we present results on the average bubble diameter, average bubble velocity, waiting time distribution between the slugs and slug frequency. The measurements were done at two different heights within the bed: $h_{low} = 70$ mm and $h_{high} = 240$ mm above the distributor plate. For AR-1 particles we investigated 5 different excess





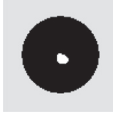

Real size:	5.2cm	2cm	5.2cm + 2cm
AR-1:			
Estimated size:	5.53cm	2.08cm	5.42cm + 2.02cm
AR-4:			
Estimated size:	5.32cm	1.96cm	5.36cm + 2.21cm

Fig. 2. Reconstructions of different combinations of phantoms in beds of AR-1 and AR-4 particles.

gas velocities: $U - U_{mf} = 0.4, 0.65, 0.9, 1.15$ and 1.4 m/s. Due to the specifics of its fluidization, AR-4 particles were fluidized at only three excess gas velocities: $U - U_{mf} = 0.6, 0.9$ and 1.15 m/s. At a gas velocity of $U - U_{mf} = 0.4$ m/s, AR-4 particles were in an active channeling regime and there were no proper bubbles or slugs forming, while at the highest gas velocity of $U - U_{mf} = 1.4$ m/s slugs of particles were lifted to the top of the column and remain stuck there, clogging the column.

As stated in Section 2.2 bubbles with an average diameter less than 2 cm are neglected in further analysis together with bubbles that are present in less than 10 frames. Measurements are done for 60 s in case of average bubble diameter and bubble velocity, while for the waiting time distribution and slug frequency measurements were run for 600 s in order to collect sufficient statistics.

3.1. Average bubble diameter

The average bubble diameter can be directly obtained from the reconstructed tomographic images. For each frame, individual bubbles are detected and their surface is calculated by summing the number of pixels that are allocated to them. A sphere-equivalent bubble diameter is calculated for each bubble and the average bubble diameter is calculated for the whole measurement. Some examples of reconstructed images and bubble visualizations are presented in Fig. 3. This is a pseudo-3D representation of reconstructed bubbles as the z-axis is a temporal and not spatial coordinate. Already from this visualizations it is clear that the fluidized beds are operating in the slugging regime. Therefore the bubble size actually refers to the slug size.

Time averaged bubble diameters for AR-1 and AR-4 particles at two heights in the bed and for different excess gas velocities are shown in Fig. 4. As the fluidized bed is operating in the slugging regime, a change

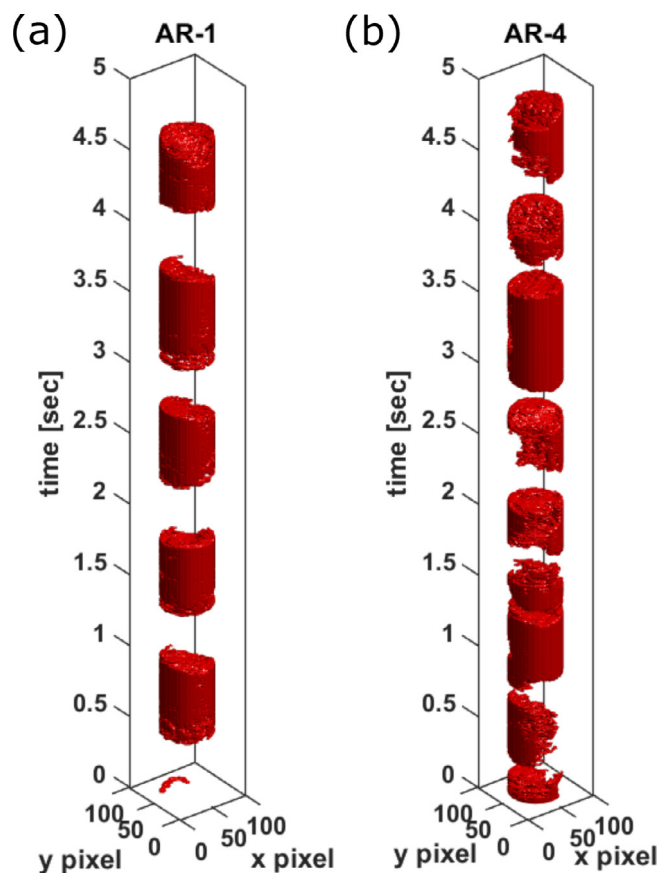


Fig. 3. Bubble visualizations for at bed height of 240 mm and $U - U_{mf} = 0.65$ m/s for (a) AR-1 and (b) AR-4 particles.

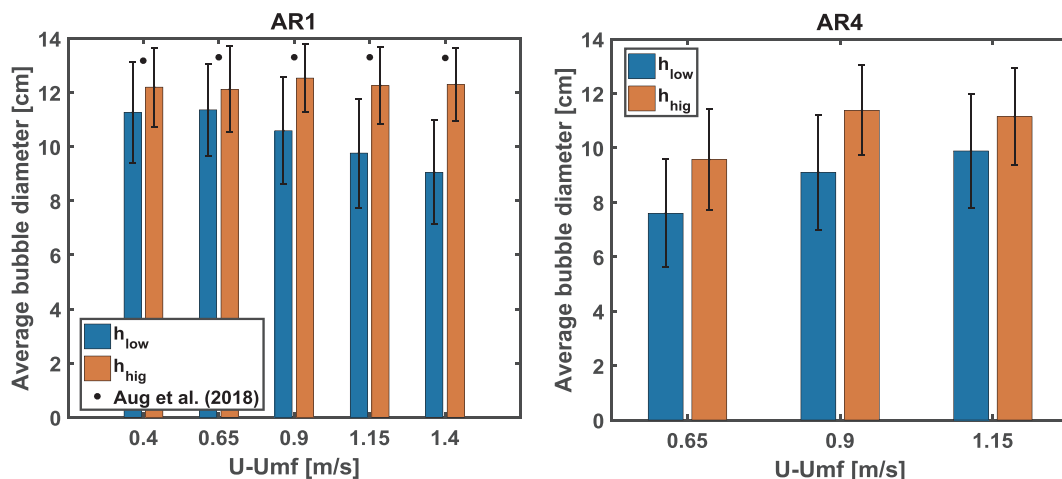


Fig. 4. Average bubble diameter for AR-1 and AR-4 particles on different excess gas velocities. Error bars indicate standard deviation of bubble diameters. The dots indicate indicate the average bubble size predicted by Aug et al. [31] for spherical (AR-1) particles in a high aspect ratio bed.

of fluid velocity does not have a considerable effect on the bubble diameter at the higher position in the bed. However it can be noticed that in all cases the average bubble diameters are smaller for the AR-4 particles than for the AR-1 particles. This can indicate that the AR-4 particles are actually slugging less and have more small and medium size bubbles. In all cases investigated, bubble diameters are larger at the higher position in the bed which is something already expected from basic theory of bubbling fluidized beds [23]. However, it is surprising that the average bubble diameter at the lower height in the bed of AR-1 particles is reducing with increasing fluid velocity.

This counter-intuitive results can be explained if we look at the average number of bubbles shown in Fig. 5. It can be seen that at high position in the reactor (red crosses), the number of bubbles remains roughly the same or shows a slight increase with an increase of gas velocity. At a low position in the reactor (blue stars), for AR-1 particles it can be seen that the decrease of average bubble diameter is accompanied by a monotonous increase of number of bubbles. On the other hand Fig. 4 shows that for AR-4 particles the average bubble diameter at the low position in the bed is increasing and from Fig. 5 it can be seen that this is accompanied by a decrease in the number of bubbles.

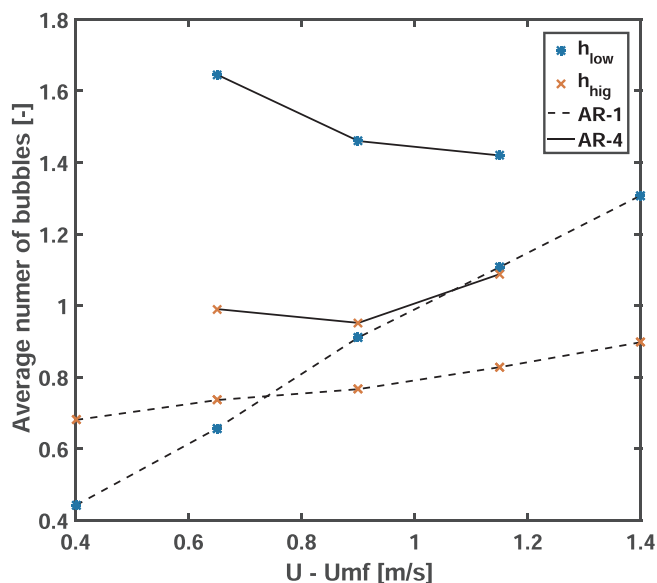


Fig. 5. Average number of bubbles present in the horizontal cross-sections at low (*) and high (x) positions in the bed, for AR-1 (- -) and AR-4 (—) particles, as a function of excess gas velocity.

A model for predicting the average bubble diameter for Geldart D type particles in the slugging regime, which was recently developed by Aug et al. [31], is the only one comparable with the fluidized bed investigated in this work. Even though this model was not tested for bed height to diameter ratios below 4 and for $U - U_{mf}$ greater than 0.4 m/s, we compare it to our experimental results for AR-1 particles in Fig. 4. This model does not depend on the height in the bed and it can be seen that it slightly overpredicts the bubble diameters, but it is still in the upper range of standard deviation at the higher position in the bed. However for AR-4 particles the model predicts fully developed slugs with diameters close to the column diameter (13.96 cm) and does not change considerably with increase of gas excess velocity, therefore it is not included in Fig. 4.

In order to get a better insight in the fluidization behavior of the considered particles, the bubble size distributions are presented in Fig. 6. The clear peak at a bubble diameter of around 13 cm indicates clear slugging behavior, knowing that the column diameter is 14 cm. It can be seen that in all cases the AR-1 particles show more extreme slugging behavior. The AR-4 particles show a much higher distribution of small and medium size bubbles compared to the AR-1 particles. The height of the peak at maximum bubble diameter is also smaller for AR-4 than AR-1 particles. At the lower position in the bed (H_{low}) it can also be noted that an increase in the gas velocity leads to an increase of the number of small and medium size bubbles for AR-1 particles, however never reaching the large number of small and medium bubbles observed for AR-4 particles. In the case of AR-4 particles, the opposite is the case: an increase of the gas velocity actually reduces the number of small and medium size bubbles while increasing the number of slugs. In summary, at the lower position in the bed, the trend of the bubble size distribution with gas velocity is opposite for AR-1 and AR-4 particles, where at high gas velocity the distribution seem to approach each other. In all cases the prevalence of medium and small size bubbles is lower at the higher position in the bed.

3.2. Bubble rise velocity

The bubble rise velocity is calculated by applying a cross-correlation between the signals at the 5th and 95th rows of pixels of the measured domain. The vertical distance of 90 pixels between the two rows corresponds to a distance of 1.26 cm. This is sufficiently large to make an accurate estimate of the bubble rise velocity, yet sufficiently small to neglect changes in bubble size (i.e. they do not grow, split or coalesce) over this distance. Details of the procedure of applying a cross-correlation function for calculating the bubble rise velocity are explained in [34].

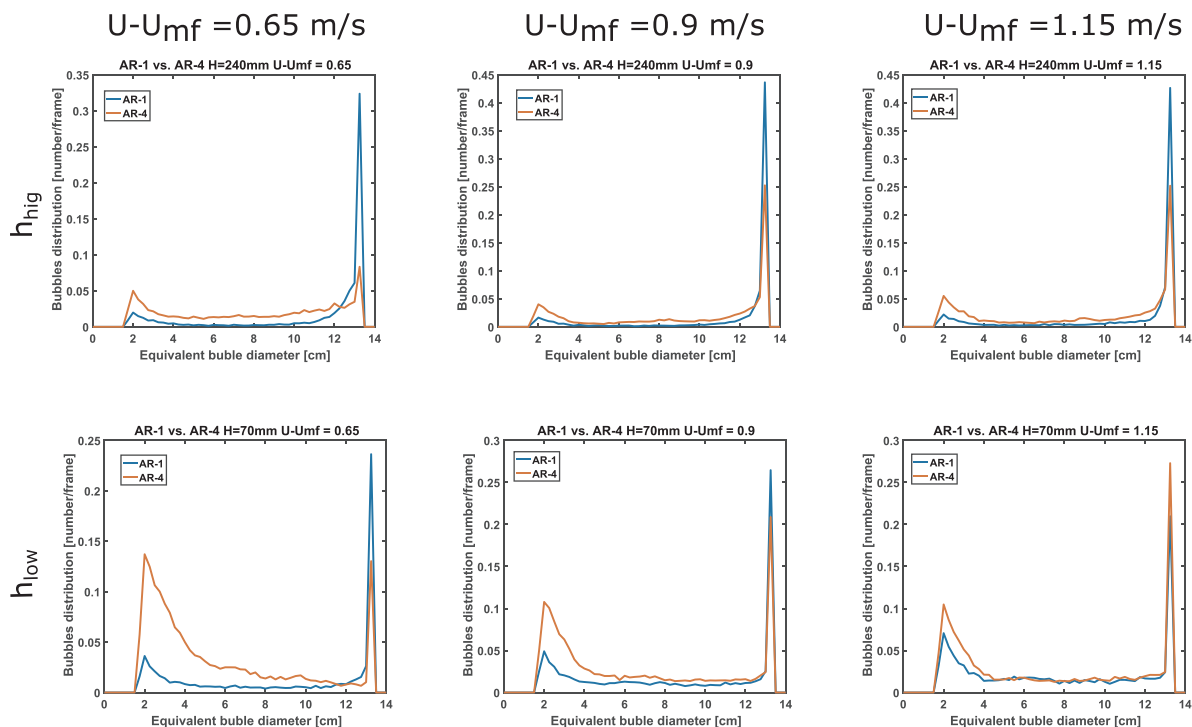


Fig. 6. Bubble size distribution for AR-1 and AR-4 particles on different excess gas velocities and low and high positions in the bed.

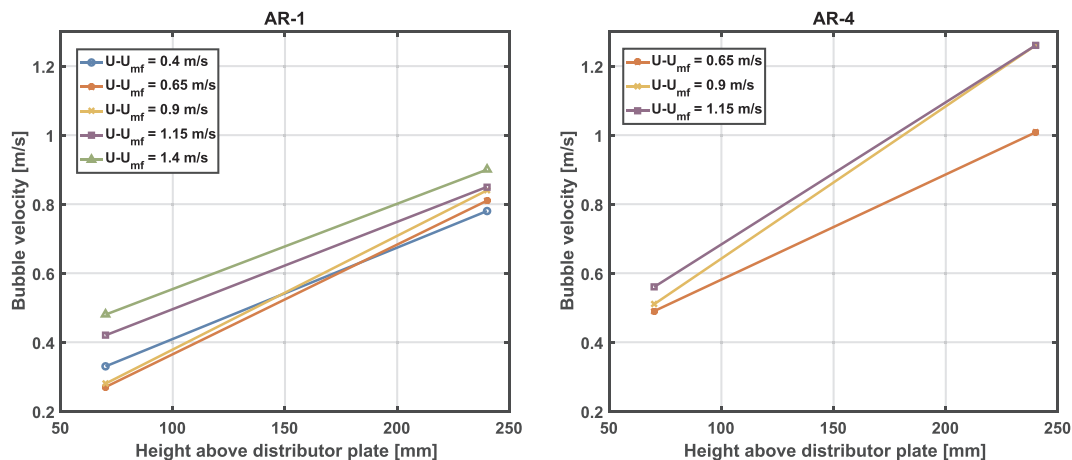


Fig. 7. Bubble velocities for AR-1 and AR-4 particles on different gas excess velocities as a function of bed height.

Fig. 7 presents the bubble rise velocities for AR-1 and AR-4 particles as a function of bed height. In all cases the bubble rise velocity is larger at the higher position in the bed and it generally increases with an increase of the gas velocity. The only exception is the slightly higher bubble rise velocity observed for AR-1 particles at the lower position in the bed at an excess gas velocity of 0.4 m/s compared to that at the next excess gas velocity of 0.65 m/s. This is caused by the presence of fewer but significantly larger bubbles at the lowest gas velocity. In the case of AR-4 particles, the bubble rise velocities are considerably higher than for AR-1 particles. This is another indication that AR-4 particles are slugging less than the AR-1 particles, because large slugs have a lower rise velocity than smaller bubbles [23].

3.3. Waiting time distribution

We now investigate the waiting time, defined as the time that passes between two consecutive slugs passing through a horizontal measurement plane. In particular, we are interested in the waiting time

distribution. The signal intensity measured on one of the detector plates is averaged over a horizontal row of pixels at the height of interest. In order to consider only slugs, and neglect small and medium size bubbles, we apply a threshold on the averaged signal intensity, as shown in Fig. 8. The waiting time is calculated as the time interval between the centers of two consecutive slugs identified through the normalized signal intensity shown in the lower images of Fig. 8. Already from the signal intensities in the upper images of Fig. 8, a clear difference between AR-1 and AR-4 particles can be seen. In the case of AR-1 particles, high intensity peaks corresponding to slugs appear regularly with almost identical distance between them. In contrast, for AR-4 particles we observe a mixture of periods with high intensity peaks and periods with smaller intensity peaks, the latter of which corresponds to small and medium bubbles passing by. Similar trends are observed for other gas excess velocities (not shown).

For brevity we present the waiting time distributions for AR-1 and AR-4 particles only at the higher position in the bed h_{high} because we find this to be the most relevant for analyzing slugging behavior. Fig. 9

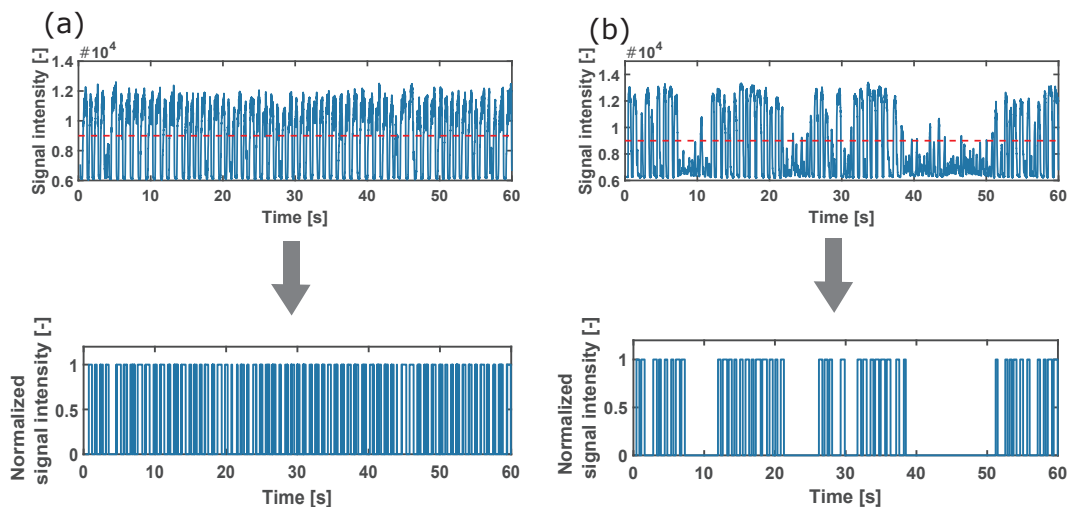


Fig. 8. Signal intensity before and after applying threshold for (a) AR-1 and (b) AR-4 particles at h_{high} and $U - U_{\text{mf}} = 0.65$ m/s.

shows quite discrete waiting time distributions for AR-1 particles. For all gas velocities there is a relatively narrow peak at a waiting time of around 1s. At the lowest gas velocity considered (Fig. 9 (a)) the main peak at 1s is followed by clear peaks at around 2, 3 and 4s. This shows that large slugs are sometimes skipped at low gas velocity, probably because a smaller slug passes by which does not overcome our threshold value for detection. With increasing the gas velocity these peaks at longer waiting times are disappearing followed by a widening of the main peak at 1s. Overall, this shows that slugs for AR-1 particles appear regularly with break of around 1s between them.

Fig. 10 shows the waiting time distributions for AR-4 particles. Notice that AR-4 particle show completely different waiting time distributions than AR-1 particles. For AR-1 particles all waiting time distributions were in range from 0.5 s up to 7.5 s, with the majority of the

distributions occurring in the range between 0.5 s and 2 s. For AR-4 particles, a much wider waiting time distribution can be seen, with peaks appearing at 12, 20 and even up to 60 s. Due to this large spread in waiting times, some of the figures in Fig. 10 are presented on a logarithmic scale for the waiting time. Clearly, there are long periods in the fluidization of AR-4 particles without appearance of slugs, but rather with medium and smaller size bubbles. This explains lower average bubble sizes and higher average number of bubbles appearing for AR-4 particles discussed in Section 3.1.

3.4. Slug frequency

The waiting time distribution discussed in the previous section indicate that there is a certain regularity in slug appearance. More

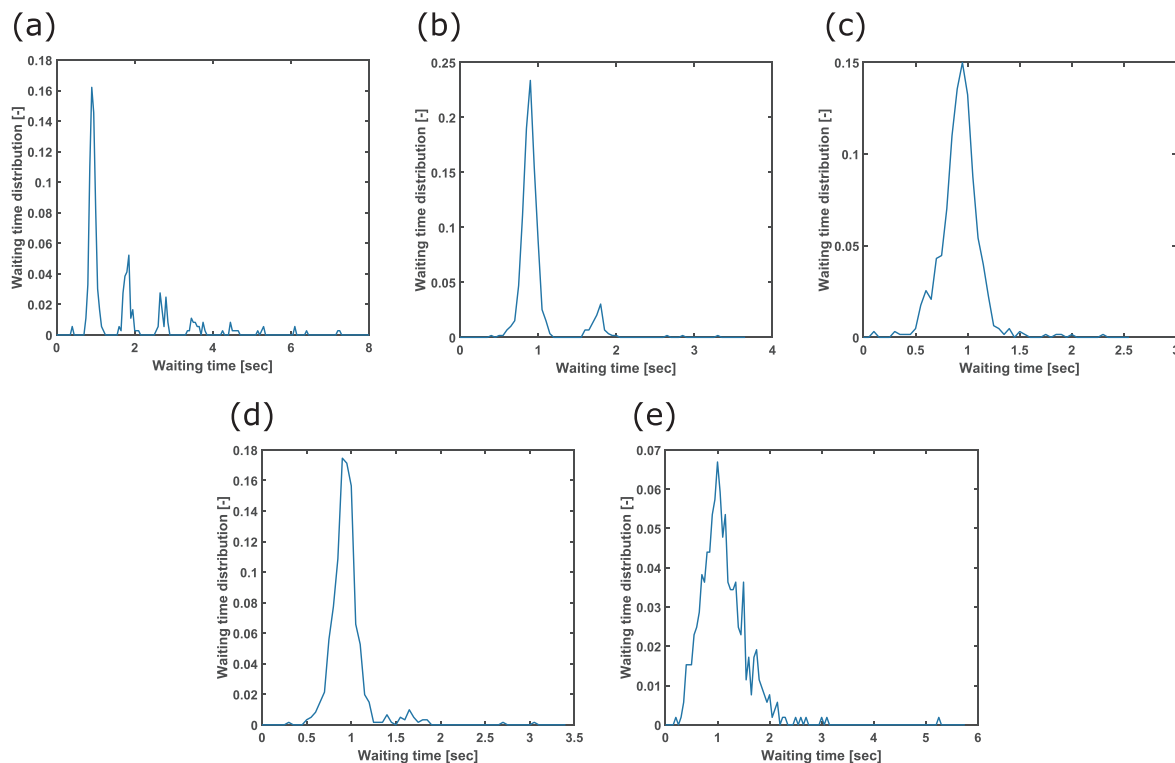


Fig. 9. Waiting time distribution for AR-1 particles at the higher bed height h_{high} and excess gas velocities $U - U_{\text{mf}}$ of: (a) 0.4, (b) 0.65, (c) 0.9, (d) 1.15 and (e) 1.4 m/s.

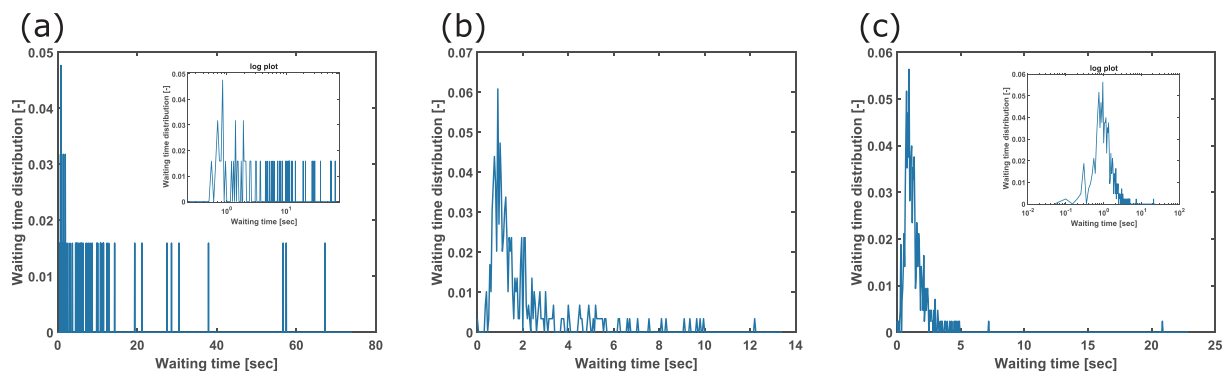


Fig. 10. Waiting time distribution for AR-4 particles at the higher bed height h_{hig} and excess gas velocities $U - U_{\text{mf}}$ of: (a) 0.65, (b) 0.9 and (c) 1.15 m/s.

information about the frequency of slugs can be obtained from a power spectrum of the signal intensity as seen in Fig. 8. The power spectrum is calculated by applying a fast Fourier transformation with a Hanning window on the normalized signal intensity. This frequency analysis is done for the same cases as the waiting time distribution discussed in Section 3.3.

The power spectra for AR-1 particles are shown in Fig. 11. As expected, a clear peak at a frequency of 1 Hz can be observed at all gas excess velocities. The dominant frequencies that can be seen in our cases are in the same range as predicted by [24]. At lower gas velocities, Fig. 11 (a) and (b) show smaller peaks at 2, 3 and 4 Hz. These peaks should be distinguished from the peaks that appear in Fig. 11 (c), but rather represent the 2nd, 3rd and 4th harmonics of the main frequency at 1 Hz. This demonstrates how regular the frequency of slug appearance actually is. With further increase of gas velocity, Fig. 11(d) and (e) shows that the main peak at 1 Hz is widening, which indicates a transition to a more turbulent fluidizing regime.

Fig. 12 shows the power spectra for AR-4 particles at different gas

excess velocities. It can be seen that frequency of slugs ranges predominantly between 0 and 2 Hz, however unlike the case of AR-1 particles no distinct peaks can be seen. This confirms that for AR-4 particles slugs do not appear as regularly as for AR-1 particles. The increased randomness in slug appearance indicates that the AR-4 fluidized bed is actually operating in a turbulent regime [26,40].

4. Discussion

In this work, we applied X-ray tomography (XRT) to investigate the differences in fluidization behavior between spherical (AR-1) and elongated (AR-4) particles. Two different bed heights were considered, together with five different excess gas velocities for spheres and three for elongated particles. As the particles used in this investigation are Geldart D particles, and the initial bed height corresponds to a deep bed, the fluidized bed was operating in a slugging regime. Even though the considered particles were volume equivalent and the initial bed heights were approximately the same, the results presented in this work

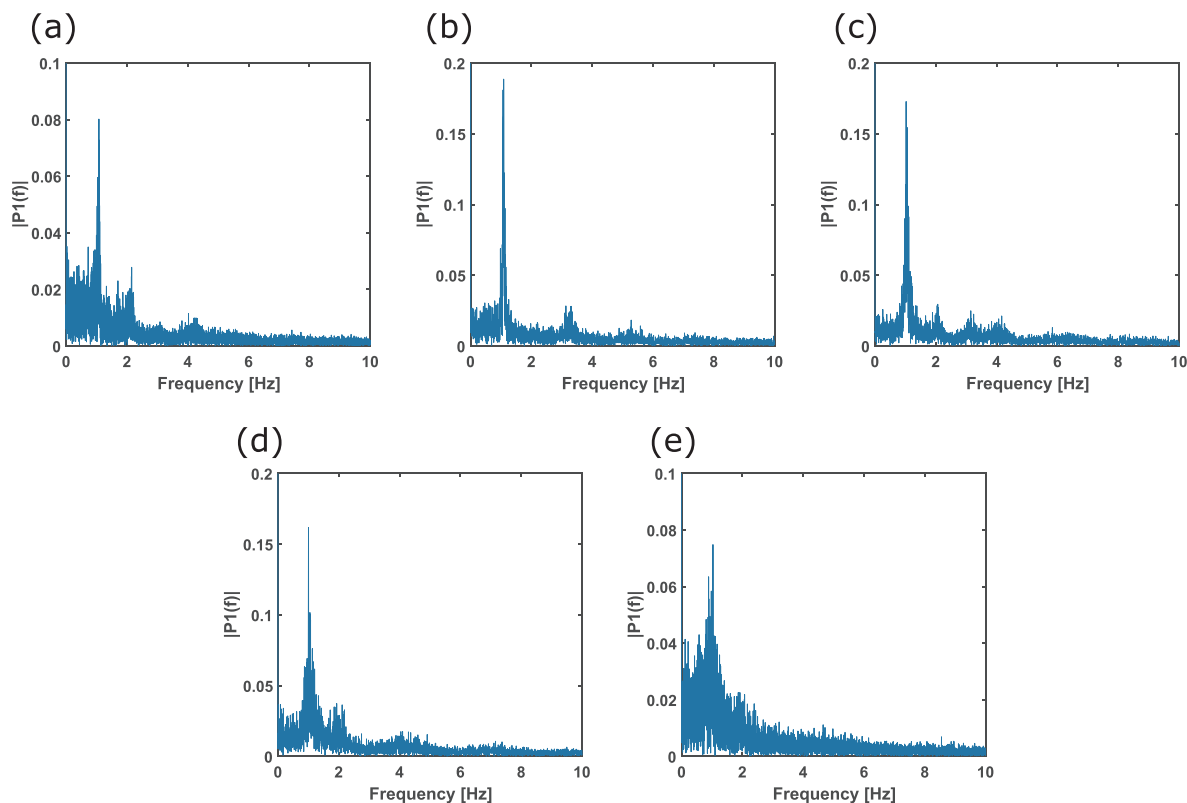


Fig. 11. Power spectra for appearance of slug for AR-1 particles at the higher bed height h_{hig} and excess gas velocities $U - U_{\text{mf}}$ of: (a) 0.4, (b) 0.65, (c) 0.9, (d) 1.15 and (e) 1.4 m/s.

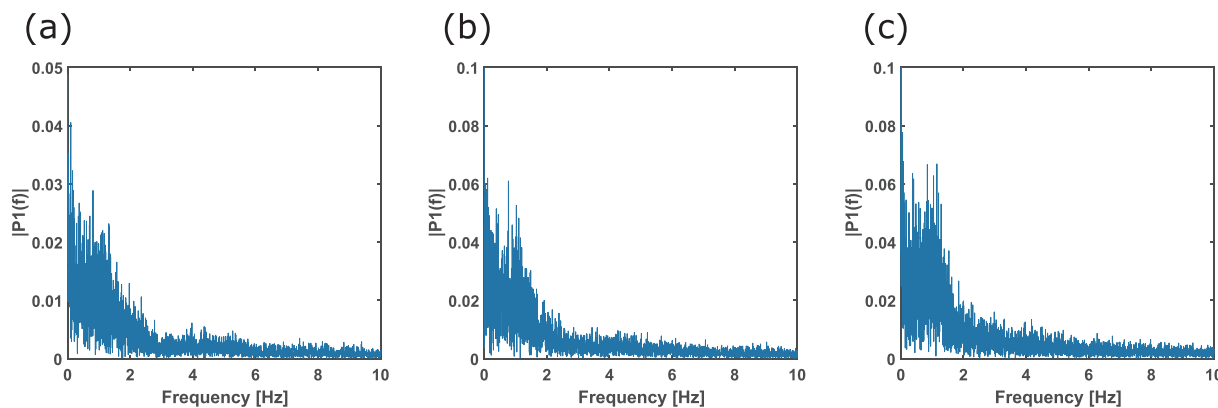


Fig. 12. Power spectra for the AR-4 particles at the higher bed height h_{high} and excess gas velocities $U - U_{\text{mf}}$ of: (a) 0.65, (b) 0.9 and (c) 1.15 m/s.

show considerably different behavior between AR-1 and AR-4 particles.

Regarding the average bubble diameter, AR-4 particles showed lower bubble sizes than AR-1 particles for all considered cases (Fig. 4), which was accompanied by a higher average number of bubbles for the case of AR-4 particles (Fig. 5). This finding was supported by the results on the bubble size distribution, which clearly showed a higher tendency for AR-1 particles to form slugs with almost no small or medium size bubbles (Fig. 6). On the other hand, AR-4 particles showed a considerably higher distribution of medium and small size bubbles. For the average bubble rise velocity, AR-4 particles showed higher values than AR-1 particles (Fig. 7). This was another indication that AR-4 particles are slugging less as smaller size bubbles have higher rise velocities than slugs [23].

The waiting time distributions between slugs and their power spectra, discussed in Sections 3.3 and 3.4 gave more insight in the periodicity and frequency of slug appearance. AR-1 particles showed a clear and narrow main peak in waiting time distribution at 1s and a corresponding dominant frequency of 1 Hz. However, the AR-4 particles waiting time distributions showed a much larger spread and the dominant peak around 1s was considerably wider than in the case of AR-1 particles. Similar behavior was noticed in the power spectra where the main frequency ranges between 1 and 2 Hz but without any clear peak of dominant frequency. This showed that once the bed of AR-1 particles is in a slugging regime, slugs appear with a quite regular frequency while AR-4 particles show much more turbulent behavior and switch between slugging and turbulent behavior [26].

Based on the results presented in this work, it can be concluded that a bed of elongated particles shows more turbulent fluidizing behavior than a bed of volume-equivalent spherical particles. With an increase of gas velocity, a slugging bed of AR-1 particles will at some point transition to turbulent fluidization [23,26]. We started to see an indication of this transition in our experiments at $U - U_{\text{mf}} = 1.4$ m/s. However for elongated AR-4 particles more turbulent fluidization can be already be seen at the lowest gas excess velocity studied. When fluidizing elongated particles, periodic transitions between slugging and turbulent fluidization can be observed. Elongated particles also show other specifics when it comes to fluidization, starting from channeling, different particle rotational velocities and solids circulation patterns, as discussed in [8,14].

We note that in this work we investigated non-spherical particles of a specific shape and aspect ratio, namely spherocylinders of aspect ratio 4. One may wonder what is the limit of aspect ratio and shape that still shows the qualitatively different fluidization behavior between non-spherical particles and spheres. We expect this limit will be for elongated particles around an aspect ratio of 2, because particle interlocking and hydrodynamic lift and torque start to play an important role for elongated particles with aspect ratios beyond approximately 2 [1,2]. However, at this point this is speculation, and more experimental work is needed to confirm this.

Applying X-ray tomography for coarse systems such as these has its limitations and challenges. Therefore we advice a certain caution when considering some of presented results. From the phantom reconstructions shown in Section 2.2 it can be seen that while the sizes of phantoms are estimated with high accuracy, the same cannot be said for their shapes. Even though we showed that small phantom with 2 cm diameter can be reconstructed with high accuracy, the high distribution of small size bubbles in Fig. 6 for AR-4 particles at low position in the bed should be interpreted with caution. Due to the higher turbulence, solid particles can be more dispersed in the gas phase and the bed shows a broader distribution of voidages, making it harder to make a clear distinction between the bubble and emulsion phases [41]. Considering all the specifics and the observed different fluidization behavior of elongated particles, we emphasize the need for better understanding and further development of numerical simulations of these kinds of systems. The results presented in this work, together with our previous findings using Magnetic particle tracking (MPT) technique [14], will be valuable for future validation of simulation results.

5. Conclusion

The results presented in this work demonstrate clear difference in fluidization behavior between spherical and elongated particles of Geldart D type. Elongated particles show a considerably larger distribution of small and medium size bubbles compared to spherical particles which show larger average bubble diameters for all gas excess velocities and bed heights considered. In all cases, elongated particles showed larger average bubble velocities. A clear difference was also observed in the waiting time distribution between slugs. In case of spherical particles, slugs appeared with more regular waiting time than elongated particles, which demonstrated a wide distribution of waiting times. Similar behavior was observed when looking into the slug frequency where spherical particles showed a clear peak at a frequency of 1 Hz, while elongated particles had a wider spread up to 2 Hz and showed no distinct peaks. All presented results indicate that elongated particles show less slugging behaviour than spherical particles and that during fluidization they periodically switch between slugging and more turbulent fluidization.

Declaration of Competing Interest

The authors declare that they have no known competing financial interests or personal relationships that could have appeared to influence the work reported in this paper.

Acknowledgments

The authors thank the European Research Council for its financial

support under its consolidator grant scheme, contract No. 615096 (NonSphereFlow).

Appendix A. Supplementary data

Supplementary data associated with this article can be found, in the online version, at <https://doi.org/10.1016/j.cej.2020.125203>.

References

- [1] S.K.P. Sanjeevi, J.T. Padding, On the orientational dependence of drag experienced by spheroids, *J. Fluid Mech.* 820. <https://doi.org/10.1017/jfm.2017.239>.
- [2] I. Mema, V.V. Mahajan, B.W. Fitzgerald, J.T. Padding, Effect of lift force and hydrodynamic torque on fluidisation of non-spherical particles, *Chem. Eng. Sci.* 195 (2019) 642–656, <https://doi.org/10.1016/j.ces.2018.10.009>.
- [3] V.V. Mahajan, T.M.J. Nijssen, J.A.M. Kuipers, J.T. Padding, Non-spherical particles in a pseudo-2d fluidised bed: Modelling study, *Chem. Eng. Sci.* 192 (2018) 1105–1123, <https://doi.org/10.1016/j.ces.2018.08.041>.
- [4] L. Seelen, J.T. Padding, J.A.M. Kuipers, A granular discrete element method for arbitrary convex particle shapes: method and packing generation, *Chem. Eng. Sci.* 189 (2018) 84–101, <https://doi.org/10.1016/j.ces.2018.05.034>.
- [5] T. Oschmann, K. Vollmari, H. Kruggel-Emden, S. Wirtz, Numerical investigation of the mixing of non-spherical particles in fluidized beds and during pneumatic conveying, *Proc. Eng.* 102 (2015) 976–985, <https://doi.org/10.1016/j.proeng.2015.01.220>.
- [6] J. Cai, Q. Li, Z. Yuan, Orientation of cylindrical particles in gas–solid circulating fluidized bed, *Particuology* 10 (1) (2012) 89–96, <https://doi.org/10.1016/j.partic.2011.03.012>.
- [7] K. Vollmari, R. Jasevičius, H. Kruggel-Emden, Experimental and numerical study of fluidization and pressure drop of spherical and non-spherical particles in a model scale fluidized bed, *Powder Technol.* 291 (2016) 506–521, <https://doi.org/10.1016/j.powtec.2015.11.045>.
- [8] V.V. Mahajan, J.T. Padding, T.M.J. Nijssen, K.A. Buist, J.A.M. Kuipers, Nonspherical particles in a pseudo-2d fluidized bed: experimental study, *AIChE J.* 64 (5) (2018) 1573–1590, <https://doi.org/10.1002/aic.16078>.
- [9] L. Boer, K.A. Buist, N.G. Deen, J.T. Padding, J.A.M. Kuipers, Experimental study on orientation and de-mixing phenomena of elongated particles in gas-fluidized beds, *Powder Technol.* 329 (2018) 332–344, <https://doi.org/10.1016/j.powtec.2018.01.083>.
- [10] M. Stein, Y. Ding, J. Seville, D. Parker, Solids motion in bubbling gas fluidised beds, *Chem. Eng. Sci.* 55 (22) (2000) 5291–5300, [https://doi.org/10.1016/S0009-2509\(00\)00177-9](https://doi.org/10.1016/S0009-2509(00)00177-9).
- [11] X. Fan, D.J. Parker, Z. Yang, J.P. Seville, J. Baeyens, The effect of bed materials on the solid/bubble motion in a fluidised bed, *Chem. Eng. Sci.* 63 (4) (2008) 943–950, <https://doi.org/10.1016/j.ces.2007.06.045>.
- [12] K.A. Buist, A.C. van der Gaag, N.G. Deen, J.A.M. Kuipers, Improved magnetic particle tracking technique in dense gas fluidized beds, *AIChE J.* 60 (9) (2014) 3133–3142, <https://doi.org/10.1002/aic.14512>.
- [13] K.A. Buist, P. Jayaprakash, J.A.M. Kuipers, N.G. Deen, J.T. Padding, Magnetic particle tracking for nonspherical particles in a cylindrical fluidized bed, *AIChE J.* 63 (12) (2017) 5335–5342, <https://doi.org/10.1002/aic.15854>.
- [14] I. Mema, K.A. Buist, J. Kuipers, J.T. Padding, Fluidization of spherical versus elongated particles - experimental investigation using magnetic particle tracking, *AIChE J.* <https://doi.org/10.1002/aic.16895>.
- [15] X. Chen, W. Zhong, T.J. Heindel, Using stereo XPTV to determine cylindrical particle distribution and velocity in a binary fluidized bed, *AIChE J.* <https://doi.org/10.1002/aic.16485>.
- [16] X. Chen, W. Zhong, T.J. Heindel, Orientation of cylindrical particles in a fluidized bed based on stereo x-ray particle tracking velocimetry (XPTV), *Chem. Eng. Sci.* 203 (2019) 104–112, <https://doi.org/10.1016/j.ces.2019.03.067>.
- [17] Y. Makkawi, P. Wright, Fluidization regimes in a conventional fluidized bed characterized by means of electrical capacitance tomography, *Chem. Eng. Sci.* 57 (13) (2002) 2411–2437, [https://doi.org/10.1016/S0009-2509\(02\)00138-0](https://doi.org/10.1016/S0009-2509(02)00138-0).
- [18] C. Rautenbach, R. Mudde, X. Yang, M. Melaen, B. Halvorsen, A comparative study between electrical capacitance tomography and time-resolved x-ray tomography, *Flow Meas. Instrum.* 30 (2013) 34–44, <https://doi.org/10.1016/j.flowmeasinst.2012.11.005>.
- [19] M. Zhang, M. Soleimani, Simultaneous reconstruction of permittivity and conductivity using multi-frequency admittance measurement in electrical capacitance tomography, *Meas. Sci. Technol.* 27 (2) (2016) 025405, <https://doi.org/10.1088/0957-0233/27/2/025405>.
- [20] T. Grassler, K.-E. Wirth, X-ray computer tomography — potential and limitation for the measurement of local solids distribution in circulating fluidized beds, *Chem. Eng. J.* 77 (1–2) (2000) 65–72, [https://doi.org/10.1016/S1385-8947\(99\)00133-3](https://doi.org/10.1016/S1385-8947(99)00133-3).
- [21] R.F. Mudde, Time-resolved x-ray tomography of a fluidized bed, *Powder Technol.* 199 (1) (2010) 55–59, <https://doi.org/10.1016/j.powtec.2009.04.021>.
- [22] T. Kai, M. Misawa, T. Takahashi, I. Tiseanu, N. Ichikawa, N. Takada, Application of fast x-ray CT scanner to visualization of bubbles in fluidized bed, *J. Chem. Eng. Japan* 33 (6) (2000) 906–909, <https://doi.org/10.1252/jcej.33.906>.
- [23] O.L.D. Kunii, Fluidization Engineering, Elsevier Science, 2013 URL: https://www.ebook.de/de/product/23543409/d_kunii_octave_levenspiel_fluidization_engineering.html.
- [24] J. Baeyens, D. Geldart, An investigation into slugging fluidized beds, *Chem. Eng. Sci.* 29 (1) (1974) 255–265, [https://doi.org/10.1016/0009-2509\(74\)85051-7](https://doi.org/10.1016/0009-2509(74)85051-7).
- [25] W.J. Thiel, O.E. Potter, Slugging in fluidized beds, *Ind. Eng. Chem. Fundamentals* 16 (2) (1977) 242–247, <https://doi.org/10.1021/i160062a012>.
- [26] S. Satija, L.-S. Fan, Characteristics of slugging regime and transition to turbulent regime for fluidized beds of large coarse particles, *AIChE J.* 31 (9) (1985) 1554–1562, <https://doi.org/10.1002/aic.690310919>.
- [27] R.D. Felice, S. Rapagnà, P. Foscolo, Dynamic similarity rules: validity check for bubbling and slugging fluidized beds, *Powder Technol.* 71 (3) (1992) 281–287, [https://doi.org/10.1016/0032-5910\(92\)88034-f](https://doi.org/10.1016/0032-5910(92)88034-f).
- [28] W. Kong, T. Tan, J. Baeyens, G. Flamant, H. Zhang, Bubbling and slugging of geldart group a powders in small diameter columns, *Ind. Eng. Chem. Res.* 56 (14) (2017) 4136–4144, <https://doi.org/10.1021/acs.iecr.6b04798>.
- [29] W. Kong, J. Baeyens, G. Flamant, T. Tan, H. Zhang, Solids flow in a “particle-in-tube concentrated solar heat absorber, *Ind. Eng. Chem. Res.* 58 (11) (2018) 4598–4608, <https://doi.org/10.1021/acs.iecr.8b04544>.
- [30] F. Sabatier, R. Ansart, H. Zhang, J. Baeyens, O. Simonin, Experiments support simulations by the NEPTUNE_CFD code in an upflow bubbling fluidized bed reactor, *Chem. Eng. J.* 385 (2020) 123568, <https://doi.org/10.1016/j.cej.2019.123568>.
- [31] C.E. Agu, C. Pfeifer, M. Eikeland, L.-A. Tokheim, B.M.E. Moldestad, Models for predicting average bubble diameter and volumetric bubble flux in deep fluidized beds, *Ind. Eng. Chem. Res.* 57 (7) (2018) 2658–2669, <https://doi.org/10.1021/acs.iecr.7b04370>.
- [32] C.E. Agu, L.-A. Tokheim, M. Eikeland, B.M. Moldestad, Improved models for predicting bubble velocity, bubble frequency and bed expansion in a bubbling fluidized bed, *Chem. Eng. Res. Des.* 141 (2019) 361–371, <https://doi.org/10.1016/j.cherd.2018.11.002>.
- [33] C.M. Venier, A.R. Urrutia, J.P. Capossio, J. Baeyens, G. Mazza, Comparing ANSYS fluent and OpenFOAM simulations of geldart a, b and d bubbling fluidized bed hydrodynamics, *Int. J. Numer. Methods Heat Fluid Flow* 30 (1) (2019) 93–118, <https://doi.org/10.1108/hff-04-2019-0298>.
- [34] V. Verma, J.T. Padding, N.G. Deen, J.A.M.H. Kuipers, F. Barthel, M. Bieberle, M. Wagner, U. Hampel, Bubble dynamics in a 3-d gas-solid fluidized bed using ultrafast electron beam x-ray tomography and two-fluid model, *AIChE J.* 60 (5) (2014) 1632–1644, <https://doi.org/10.1002/aic.14393>.
- [35] S.M. Maurer, D. Gschwend, E.C. Wagner, T.J. Schildhauer, J.R. van Ommen, S.M. Biollaz, R.F. Mudde, Correlating bubble size and velocity distribution in bubbling fluidized bed based on x-ray tomography, *Chem. Eng. J.* 298 (2016) 17–25, <https://doi.org/10.1016/j.cej.2016.02.012>.
- [36] J. Ma, J.R. van Ommen, D. Liu, R.F. Mudde, X. Chen, E.C. Wagner, C. Liang, Fluidization dynamics of cohesive geldart b particles. part i: X-ray tomography analysis, *Chem. Eng. J.* 359 (2019) 1024–1034, <https://doi.org/10.1016/j.cej.2018.11.082>.
- [37] S. Jahangir, E.C. Wagner, R.F. Mudde, C. Poelma, Void fraction measurements in partial cavitation regimes by x-ray computed tomography, *Int. J. Multiph. Flow* 120 (2019) 103085, <https://doi.org/10.1016/j.ijmultiphaseflow.2019.103085>.
- [38] S. Maurer, E.C. Wagner, J.R. van Ommen, T.J. Schildhauer, S.L. Teske, S.M. Biollaz, A. Wokaun, R.F. Mudde, Influence of vertical internals on a bubbling fluidized bed characterized by x-ray tomography, *Int. J. Multiph. Flow* 75 (2015) 237–249, <https://doi.org/10.1016/j.ijmultiphaseflow.2015.06.001>.
- [39] X. Yang, J.R. van Ommen, J. Schoormans, R.F. Mudde, A hybrid tomographic reconstruction algorithm for high speed x-ray tomography, *Comput. Phys. Commun.* 196 (2015) 27–35, <https://doi.org/10.1016/j.cpc.2015.05.010>.
- [40] B. Du, L.-S. Fan, F. Wei, W. Warsito, Gas and solids mixing in a turbulent fluidized bed, *AIChE J.* 48 (9) (2002) 1896–1909, <https://doi.org/10.1002/aic.690480907>.
- [41] N. Ellis, L. Briens, J. Grace, H. Bi, C. Lim, Characterization of dynamic behaviour in gas–solid turbulent fluidized bed using chaos and wavelet analyses, *Chem. Eng. J.* 96 (1–3) (2003) 105–116, <https://doi.org/10.1016/j.cej.2003.08.017>.